Visualization of static Jahn-Teller effects in the fullerene anion C_{60}^-

Ian D. Hands, Janette L. Dunn,[*] and Colin A. Bates

School of Physics and Astronomy, University of Nottingham, Nottingham NG7 2RD, United Kingdom
(Received 21 July 2010; published 15 October 2010)

Adsorption of C_{60} on a metallic surface may be expected to result in electronic charge transfer to the organic adsorbant, even if a buffer layer is included between the C_{60} molecules and substrate. Subsequently, intramolecular coupling between the molecule's electronic and vibrational degrees of freedom would be expected to result in species subject to Jahn-Teller (JT) distortions. In this work, we use Hückel molecular-orbital theory to visualize the effect that JT interactions may have on C_{60}^- ions imaged using scanning tunneling microscopy (STM). Several distortion symmetries and adsorption orientations are considered and the resulting simulations are compared to STM images in the literature.

I. INTRODUCTION

Since its development nearly three decades ago,[1,2] scanning tunneling microscopy (STM) has blossomed into a powerful tool for imaging molecular orbitals (MOs) with atomic resolution.[3,4] Positive sample biases permit images to be obtained of unoccupied orbitals, usually of the lowest unoccupied MO (LUMO) while negative biases generate an image from the filled states, usually of the highest occupied MO (HOMO).

STM of the fullerene molecule C_{60} is particularly interesting for several reasons. Due to the large size of the molecule, high-resolution (HR) STM is capable of resolving intramolecular features. When adsorbed on a surface, STM allows the adsorption geometry to be identified, as well as the effects of interactions with the surface to be probed. The high symmetry of the C_{60} molecule means that the molecular orbitals of the free molecule are highly degenerate, with the LUMO belonging to the T_{1u} icosahedral irrep and the HOMO belonging to the H_u irrep. This degeneracy cannot be maintained on the surface as inversion symmetry must be necessarily absent. In a recent paper,[5] the effects of the loss of degeneracy due to surface adsorption on the appearance of the molecule, as observed using STM, were explored theoretically. Various images were inferred, several of which compare very well with features observed in actual STM work.

Another reason for interest in the C_{60}-surface system is that there may be signatures in the STM images that arise from electron-phonon coupling. It has been suggested that STM images of C_{60} molecules codeposited onto a gold surface with potassium[6] give direct evidence for the occurrence of a static intramolecular Jahn-Teller (JT) effect. Such vibronic interactions in C_{60} have been of great interest since the first discovery that bulk fullerides of the form A_3C_{60} (where A is an alkali metal) become superconducting at relatively high temperatures.[7,8] This superconductivity may, in part, be due to vibronic coupling[9] and so any observation of the JT effect in fulleride ions could be potentially important. Therefore, identification and quantification of the strength of the vibronic coupling in surface-adsorbed monolayers (MLs) of C_{60} using STM may provide information that has important ramifications for superconductivity in their bulk counterparts.

In order to extract reliable information from STM images about the nature of vibronic coupling, it is necessary to have a good understanding of many factors which influence the appearance of the image. This includes the interplay between intramolecular JT effects, surface interactions, orientational ordering, and intramolecular interactions with neighboring ions (such as in the cooperative JT effect), and charge transfer (CT) effects. This leads to a very complicated picture indeed. Therefore, in this paper, we will concentrate on the effects intramolecular JT coupling and surface interactions have on observed STM images of C_{60}^- anions adsorbed on surfaces. Our results will permit understanding of the subtle behavior often engendered by the JT effect without having to become entangled with the complex methods used to deal with the JT states involved. With this in mind, we have actively sought to keep the current work as clear of as much mathematical detail as possible. While our principal aim is not to model observed experimental results, some of the features we illustrate will appear in real STM experiments, as we will discuss later.

Any intramolecular JT treatment itself is nontrivial. First, there is the need to know the charge of the ion with which we are concerned. This will be affected by the degree of doping, and any surface-induced charge transfer that may be present even in the absence of any doping. Second, for C_{60}^{n-} ions, where $n=2-6$, there will be additional effects due to Coulombic electron-electron interactions, which are not well quantified themselves. Also, the vibronic coupling in any of the C_{60} anions is complicated because of the large number of normal modes. Thus even the relatively simple ion C_{60}^- is subject to an eight mode $T_{1u} \otimes 8h_g$ JT effect arising from the eight normal modes of h_g symmetry. Each mode requires one linear coupling constant to quantify its effect on the system and inclusion of higher order coupling effects will rapidly make this worse. For instance, accounting for quadratic coupling requires a further two additional coupling constants for each mode (because $h \otimes h$ is nonsimply reducible). Nevertheless, for many purposes it is possible to treat JT problems involving multiple modes in terms of a single effective mode.[10] An effective mode treatment can be expected to apply to the determination of the general features of the effect of JT coupling on STM images because strong bonding within the C_{60} cage structure will result in distorted struc-

tures in which the individual carbon atoms have only moved very small distances from their positions in the undistorted (icosahedral) molecule. For imaging purposes, the molecular structure can be effectively fixed in an icosahedral geometry. The JT effects detected, therefore, are those attributable to changes in the electronic components of the vibronic states. This means that the actual h_g mode(s) used to model the distortion become irrelevant.

Next, we must realize that the STM technique itself operates on a relatively slow (millisecond) time scale. As a rough guide, a fast scan (as used to form a series of snapshots of a Pt surface to illustrate real-time diffusion[11]) corresponds to imaging a 140×140 Å^2 area in approximately 13 s. For a C_{60} molecule with a diameter of 7 Å, this corresponds to a dwell time of ~ 33 ms. At sufficiently low temperatures, the usual translational, vibrational, and rotational degrees of freedom clearly become suppressed to a degree that has allowed intramolecular detail to be discerned in STM images of surface-adsorbed C_{60}. Thus, STM is a fast-enough technique to freeze normal molecular motion. However, it is not clear that this is still the case if the additional dynamical behavior associated with the JT effect is present.

For a highly symmetric molecule like C_{60}, the JT effect[12] produces a set of distorted atomic arrangements corresponding to minimum-energy points in the adiabatic potential-energy surface (APES). Each arrangement appears identical except for its orientation and so we will refer to them here as "orientomers." Each orientomer is of lower symmetry than the original icosahedral C_{60} molecule. For C_{60}^- anions, this could result in six D_{5d}, ten D_{3d}, 14 D_{2h}, or 30 C_{2h} orientomers, depending on the vibronic coupling present. Each configuration has the same energy and so, when there is no additional perturbation, the system may become localized in any one of the equivalent arrangements of a given symmetry. The potential barriers between orientomers are finite and so tunneling between them will occur. This leads to a unique dynamical motion referred to as pseudorotation (which can be viewed as being the rotation of a distortion). The rate at which pseudorotation occurs, or equivalently, the rate at which the system "hops" between potential minima, defines a new time scale which depends ultimately on the strength of the vibronic coupling present.[13–15]

Observing a dynamic JT system via STM necessarily means that the image recorded will depend on the relative magnitudes of the two time scales involved. Let us suppose that the system spends on average around 330 ms in a particular well, that is, ten times the amount of time that might be required to obtain an STM image from the system using the fastest apparatus mentioned earlier. This eventuality could then, justifiably, be labeled as observation of a "static" JT effect. Further, suppose that the effective frequency of the coupled motion corresponds to an average C_{60} vibrational energy of 500 cm^{-1} ($\omega \sim 9.4 \times 10^{13}$ s). Taking the 330 ms time scale to represent the pseudorotational period, this means that the required dimensionless pseudorotational rate, as defined in Ref. 14, is $\mathcal{R}^{(p)} \approx 2 \times 10^{-13}$. When second-order effects are neglected, the results in Ref. 14 suggest that this slow rate of pseudorotation requires an eightfold larger degree of linear vibronic coupling than suggested by experiment,[16,17] and also a much larger degree than suggested by calculation.[18–22]

Including quadratic JT effects could reduce the value of linear coupling needed to observe images that appear static on the STM time scale. Even in this case the picture is not simple. Each of the orientomers will have the same energy (still assuming any other perturbations are weak) and so the probability of observing any particular orientomer will be the same. If we assume that every C_{60} molecule adsorbs onto the surface with the same orientation, then we need to know what each orientomer would look like if viewed via STM. Energywise, each of these different images will appear at the same applied bias and so a ML of identical units would be expected to produce a rather complicated pattern of different images. In fact, as the magnitudes of the quadratic constants could be expected to be small, it seems unlikely that JT effects alone could localize the system into a single orientomer on an STM time scale. Thus, it seems that captured STM images would be a composite of images arising from all of the equivalent wells, and possibly with some contribution from other regions of the pseudorotation path.

If we include additional interactions, such as intermolecular JT effects or surface interactions, the degeneracy of the orientomers could be lifted. It is then possible that the system could be localized into one particular orientomer to such an extent that the STM effectively captures a snapshot of that orientomer alone. Alternatively, the surface interaction could favor a subset of orientomers such that the observed STM image would be a superposition of a smaller subset of images. This would greatly simplify the appearance of a ML film.

Despite the problems associated with time scales, multiple competing interactions, orientation, and lack of knowledge of key parameters needed to model C_{60} anions, it is clear that a careful and methodical use of STM imaging could yield valuable information about the JT effect in such molecules. Correspondingly, it is important that comprehensive theoretical work be undertaken to help disentangle the complex images that may be observed, and to thus derive useful information about the JT effect and other interactions present. This is attempted in this paper for the case of C_{60}^- anions.

The starting point for our method is to use Hückel MO (HMO) theory to generate the orbitals to be imaged rather than the more usual density-functional theory (DFT). While DFT does undoubtedly give good results for this system, it is computationally expensive to implement. Using HMOs allows us to obtain images for a wide range of different situations very quickly on a standard personal computer. We took a similar approach in a recent paper relating to neutral C_{60} molecules adsorbed onto a surface (where JT effects can be ignored), where we modeled the HOMO, LUMO, and LUMO+1.[5] We obtained simulated STM images that are almost identical to those obtained using DFT. The work in this paper amplifies upon the first steps made to incorporate the JT effect into the LUMO that was taken in Ref. 23.

II. IMAGING C_{60}^-

In the monoanion C_{60}^-, the added electron resides in the T_{1u} LUMO of C_{60}. The work here will concentrate solely on this orbital. The system Hamiltonian will be written in the form

$$\mathcal{H} = \mathcal{H}_{JT} + \mathcal{H}_S, \tag{1}$$

where $\mathcal{H}_{JT}$ represents the JT Hamiltonian and $\mathcal{H}_S$ the surface interaction. The JT Hamiltonian describing coupling between the T_{1u} electronic states and a set of (effective) fivefold degenerate h_g vibrational levels can be further written in the form

$$\mathcal{H}_{JT} = \mathcal{H}_{vib} + \mathcal{H}_1 + \mathcal{H}_2 + \mathcal{H}_3, \tag{2}$$

where $\mathcal{H}_1$ is the linear JT interaction Hamiltonian, $\mathcal{H}_2$ and $\mathcal{H}_3$ are two distinct quadratic interaction Hamiltonians (arising because $h \otimes h$ contains $2h$), and $\mathcal{H}_{vib}$ is the vibrational Hamiltonian. Explicit forms for each of the Hamiltonians may be found in Ref. 24, along with explicit expressions for the vibronic states corresponding to the minima of D_{5d} or D_{3d} symmetry in the lowest APES. They also allow the positions of minima of D_{2h} or C_{2h} symmetry to be found. The energies of the minima and their ranges of validity are given in the Appendix.

In Ref. 5, the surface interaction $\mathcal{H}_S$ was treated thoroughly using group theoretical methods. However, in this paper we will take the JT effect to be of most importance and treat the surface interaction as a secondary effect. This will be appropriate where the C_{60} molecule is physisorbed on the surface such that it essentially retains its icosahedral character. The form of $\mathcal{H}_S$ will clearly depend on the orientation with which the anion is adsorbed onto the surface. We will adopt a simple form for $\mathcal{H}_S$ used in an earlier work[23] which essentially treats the surface as a flat, featureless plane and splits the orbitals into one unique orbital associated with the normal to the surface and two degenerate ones parallel to the surface. The appropriate form can be written in the usual electronic basis $\{T_{1ux}, T_{1uy}, T_{1uz}\}$ as

$$\mathcal{H}_S = -\frac{\Delta_S(\phi)}{6} \begin{bmatrix} 1 - 3\cos 2\phi & 0 & 3\sin 2\phi \\ 0 & -2 & 0 \\ 3\sin 2\phi & 0 & 1 + 3\cos 2\phi \end{bmatrix}, \tag{3}$$

where ϕ is a single orientation-determining parameter, defined to be the angle from a C_2 symmetry axis toward C_5 and C_3 axes, as shown in Fig. 1. For the current work we will concentrate on the three possible orientations corresponding to adsorption with a double bond, pentagonal face, and hexagonal face prone to the surface, which corresponds to $\phi = 0°$, $31.72°$, and $69.09°$, respectively. It also allows us to choose other orientations that are likely to occur, e.g., a single bond, or even an individual atom, pointing toward the surface, although these cases will not be considered here.

The overall magnitude of the surface interaction is governed by the parameter Δ_S, which is taken to be a function of ϕ. The eigenvalues of $\mathcal{H}_S$ are $-2\Delta_S/3$ (singly degenerate) and $\Delta_S/3$ (doubly degenerate) and so the quantity Δ_S represents the splitting induced in the LUMO by the surface. The sign of Δ_S may be positive or negative depending on the order of the split orbitals.

III. REFERENCE GEOMETRY: ICOSAHEDRAL C_{60}^-

Before we start considering the effects of JT and surface interactions in C_{60}^-, we will discuss what could be expected
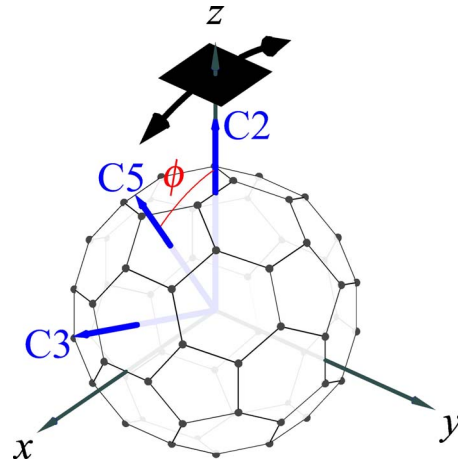

FIG. 1. (Color online) Definition of the adsorption angle ϕ. The black square (at $\phi=0$ here) represents the region of space scanned by the STM tip, so the surface is parallel to it but on the opposite side of the molecule. The labels Cn are used to denote n-fold symmetry axes.

to arise from a reference geometry corresponding to an anion free of both JT and surface interaction, where the T_{1u} orbitals are degenerate. As these orbitals are singly occupied, the ion is expected to be conducting and the STM images obtained using small positive or negative biases should be identical. Using the methods and parameters provided in earlier work[5,23] we can derive simple pictures for the total electron-density imaged, and for the expected, high-resolution STM images that would result from that electron distribution. The results for the electron density and for the STM simulation obtained for an ion adsorbed with a C_2 axis normal to the surface are given in Fig. 2. Images for other orientations can be obtained simply by an appropriate rotation of the image in Fig. 2(b), giving a fivefold ring facing forward for adsorption with a C_5 axis normal to the surface, and the midpoint between three fivefold rings facing forward for adsorption with a C_3 axis normal to the surface.

Note that Fig. 2(b) is not intended to represent a realistic STM simulation that accurately reflects data collected using a real STM device. Rather, we use parameters (e.g., high-
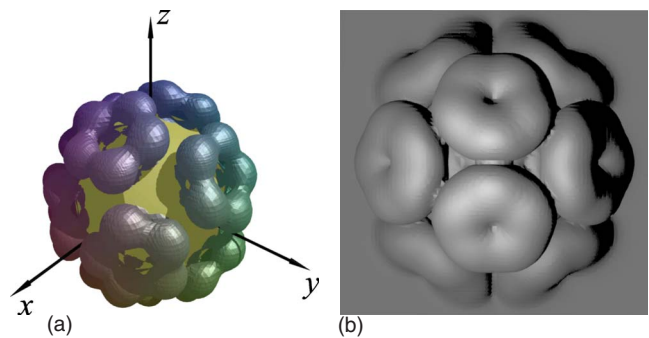

FIG. 2. (Color online) The electron distribution associated with the fully degenerate LUMO of C_{60}. (a) shows that the electrons are localized on the pentagonal faces, and (b) shows a high-resolution STM simulation for an ion adsorbed with a C_2 axis normal to the surface in the absence of JT and surface interactions.

TABLE I. Ground and excited electronic states (GS and ES, respectively) corresponding to GS minima belonging to different distortion symmetries. The basis used is $\{T_{1ux}, T_{1uy}, T_{1uz}\}$ and $\tau = (1+\sqrt{5})/2$ is the golden mean. Note that the occurrence of D_{2h} minima requires the presence of very strong quadratic coupling in this system. The states are not necessarily normalized and braces indicate degeneracy. The D_{2h} ESs are generally nondegenerate and have been written in a consistent order, i.e., the first ES in each case corresponds to the same energy (as they are symmetry related). The labels used for the minima match those used in earlier work (Refs. 24 and 25).

	D_{5d}			D_{3d}			D_{2h}	
Label	GS[a]	ES	Label	GS[a]	ES	Label	GS[b]	ES
A	$(0,\tau,1)$	$\{(1,0,0),(0,1,-\tau)\}$	a	$(0,\tau^{-1},\tau)$	$\{(1,0,0),(0,-\tau,\tau^{-1})\}$	A	$(0,0,1)$	$(1,0,0),(0,1,0)$
B	$(0,-\tau,1)$	$\{(1,0,0),(0,1,\tau)\}$	b	$(0,-\tau^{-1},\tau)$	$\{(1,0,0),(0,\tau,\tau^{-1})\}$	B	$(\tau^{-1},1,\tau)$	$(1,-\tau,\tau^{-1}),\ (\tau,\tau^{-1},-1)$
C	$(1,0,\tau)$	$\{(0,1,0),(-\tau,0,1)\}$	c	$(\tau,0,\tau^{-1})$	$\{(0,1,0),(\tau^{-1},0,-\tau)\}$	C	$(\tau^{-1},-1,\tau)$	$(1,\tau,\tau^{-1}),\ (-\tau,\tau^{-1},1)$
D	$(1,0,-\tau)$	$\{(0,1,0),(\tau,0,1)\}$	d	$(\tau,0,-\tau^{-1})$	$\{(0,1,0),(\tau^{-1},0,\tau)\}$	D	$(-\tau^{-1},-1,\tau)$	$(-1,\tau,\tau^{-1}),\ (\tau,\tau^{-1},1)$
E	$(\tau,1,0)$	$\{(0,0,1),(1,-\tau,0)\}$	e	$(\tau^{-1},\tau,0)$	$\{(0,0,1),(-\tau,\tau^{-1},0)\}$	E	$(-\tau^{-1},1,\tau)$	$(1,\tau,-\tau^{-1}),\ (\tau,-\tau^{-1},1)$
F	$(-\tau,1,0)$	$\{(0,0,1),(1,\tau,0)\}$	f	$(-\tau^{-1},\tau,0)$	$\{(0,0,1),(\tau,\tau^{-1},0)\}$	F	$(-\tau,\tau^{-1},1)$	$(\tau^{-1},-1,\tau),\ (1,\tau,\tau^{-1})$
			g	$(1,1,1)$	$\{(-2,1,1),(0,1,-1)\}$	G	$(\tau,\tau^{-1},1)$	$(-\tau^{-1},-1,\tau),\ (1,-\tau,-\tau^{-1})$
			h	$(-1,1,1)$	$\{(2,1,1),(0,1,-1)\}$	H	$(\tau,-\tau^{-1},1)$	$(-\tau^{-1},1,\tau),\ (1,\tau,-\tau^{-1})$
			i	$(1,-1,1)$	$\{(1,2,1),(1,0,-1)\}$	I	$(\tau,\tau^{-1},-1)$	$(\tau^{-1},1,\tau),\ (1,-\tau,\tau^{-1})$
			j	$(1,1,-1)$	$\{(1,1,2),(1,-1,0)\}$	J	$(1,\tau,-\tau^{-1})$	$(\tau,-\tau^{-1},1),\ (-\tau^{-1},1,\tau)$
						K	$(-1,\tau,\tau^{-1})$	$(\tau,\tau^{-1},1),\ (\tau^{-1},1,-\tau)$
						L	$(1,\tau,\tau^{-1})$	$(-\tau,\tau^{-1},1),\ (\tau^{-1},-1,\tau)$
						M	$(-1,\tau,-\tau^{-1})$	$(\tau,\tau^{-1},-1),\ (\tau^{-1},1,\tau)$
						N	$(0,1,0)$	$(0,0,1),(1,0,0)$
						O	$(1,0,0)$	$(0,1,0),(0,0,1)$

[a]From Ref. 24.
[b]From Ref. 25. Note that a $\{T_{1g}, T_{2g}, G_g\}$ basis was used in that work, as required for a C_{60}^{2+} cation. Only the T_1 part is used here.

tunneling current, arbitrarily sharp STM tip, etc.) that produce images that give a good "picture" of the electron density responsible for the image.[5,23] Thus, our images should be thought of as representing the optimum possible image quality that could be recorded using STM. It is always possible to downgrade these high-resolution images. Hence, in Fig. 2(b) a more realistic impression of what would be imaged via STM can be achieved by ignoring all but the uppermost two lobes of the image. In fact, simulations using smaller tunneling currents pick out just the central parts of Fig. 2(b), producing a two-lobed image which strongly resembles images observed in actual experiments (see Refs. 5 and 23 for details and further comparisons).

IV. STATIC JAHN-TELLER DISTORTIONS

We now examine what effects could be produced due to loss of degeneracy via a JT effect that is sufficiently strong to lock an ion into one particular potential well for a period of time that is long on the time scale of the STM data collection. This static JT effect will remove the degeneracy of the T_{1u} orbitals and thus affect the STM image shown in Fig. 2. For each minimum in the APES, the ground state (GS) will be nondegenerate and singly occupied while the excited state (ES) will be empty and either singly or doubly degenerate. Thus, we need to construct at least two images for each well considered. In order to alleviate the rapidly increasing number of simulations required, we attempt to simplify the prob-

lem by invoking the stabilizing effect of the surface. Also, to help systematize the information that is presented, we shall consider the three different types of distortion separately.

To define the labeling used here, the electronic states corresponding to the critical points in the ground APES for the three different symmetry groups are shown in Table I. Also shown are the corresponding states for the excited APESs. The primary use of the states in the table is to generate the STM simulations that follow. However, we can also plot the coordinates of the electronic ground states and their inversions through the origin to obtain a visual representation of the relative positions of the wells in the three-dimensional electronic space, as shown in Fig. 3. In these figures, we have also included an indication of the variation in potential energy of the system corresponding to the electronic states. Relating these results to Fig. 1, we can see that as ϕ varies from 0° to 90° we will start at the position of well A of the D_{2h}-distorted configuration and pass through the position of well C of the D_{5d}-distorted configuration and then well c of the D_{3d} configuration.

We can also use the states in Table I to gain an insight into the effect of the surface interaction. To do this, we treat $\mathcal{H}_S$ in Eq. (1) as a perturbation to the JT Hamiltonian so that the zeroth-order states correspond to the electronic states in Table I. The first-order correction to the energy of the system can then be found by taking the appropriate integral. For example, in a D_{5d} distortion, the energy change in well C is found to be
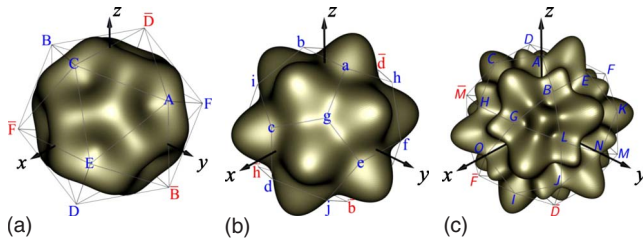
FIG. 3. (Color online) Pictorial representation of the electronic coordinates of the wells of (a) D_{5d}, (b) D_{3d}, and (c) D_{2h} symmetries. The nonbarred letters (blue online) correspond to the wells labeled as in Table I and their inverted counterparts are distinguished using an overbar (red online). The surfaces shown are intended to convey an indication of the potential energy of the system corresponding to those electronic states.

$$\Delta E_C = \langle C | \mathcal{H}_S | C \rangle / \langle C | C \rangle$$

$$= -\frac{\Delta_S}{6}\left[1 + \frac{3}{\sqrt{5}}(\cos 2\phi + 2 \sin 2\phi) \right], \quad (4)$$

where $\langle C |$ is the electronic state $(1, 0, \tau)$ as defined in Table I and $\mathcal{H}_S$ is given by Eq. (3). Thus, we can evaluate how the surface interaction favors different wells for different adsorption orientations ϕ. This allows us to just focus on a representative subset of wells, as we consider next.

A. D_{5d} distortion

For an isolated C_{60}^- ion distorted to D_{5d} symmetry by the JT effect, there are six equivalent orientomers, corresponding to the D_{5d} wells listed in Table I. The first-order corrections
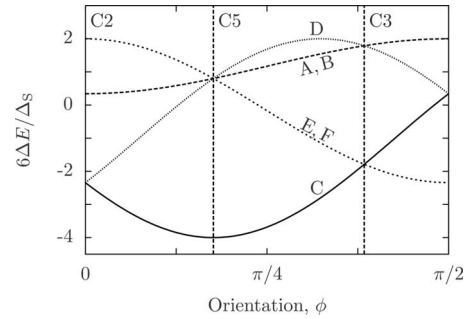

FIG. 4. The effect on the surface interaction energy for each D_{5d} well of varying the adsorption angle ϕ.

to the energies of the minima when the molecule is adsorbed onto a surface are shown in Fig. 4. It is seen that for a particular choice of adsorption orientation, the surface interaction will favor different wells, although in most cases there are still wells that are equivalent. For example, with the pentagonal face associated with well C oriented toward the surface (with ϕ taking the value C5 marked in the figure), wells A, B, D, E, and F are all still equivalent. This is consistent with Fig. 3(a), where all of these wells can be seen to be symmetrically situated with respect to well C. In this case, we can image the system as if it were locked in well C only if Δ_S is positive, or as if it is locked in any one of the remaining D_{5d} wells if Δ_S is negative—the image produced if the system were localized in one of the other wells will be the same apart from its orientation.

In all, we can see that there are 12 unique simulations required to image the ground and excited states of molecules adsorbed with C_2, C_3, or C_5 axes perpendicular to the surface, as shown in Fig. 5. The images give a complete picture
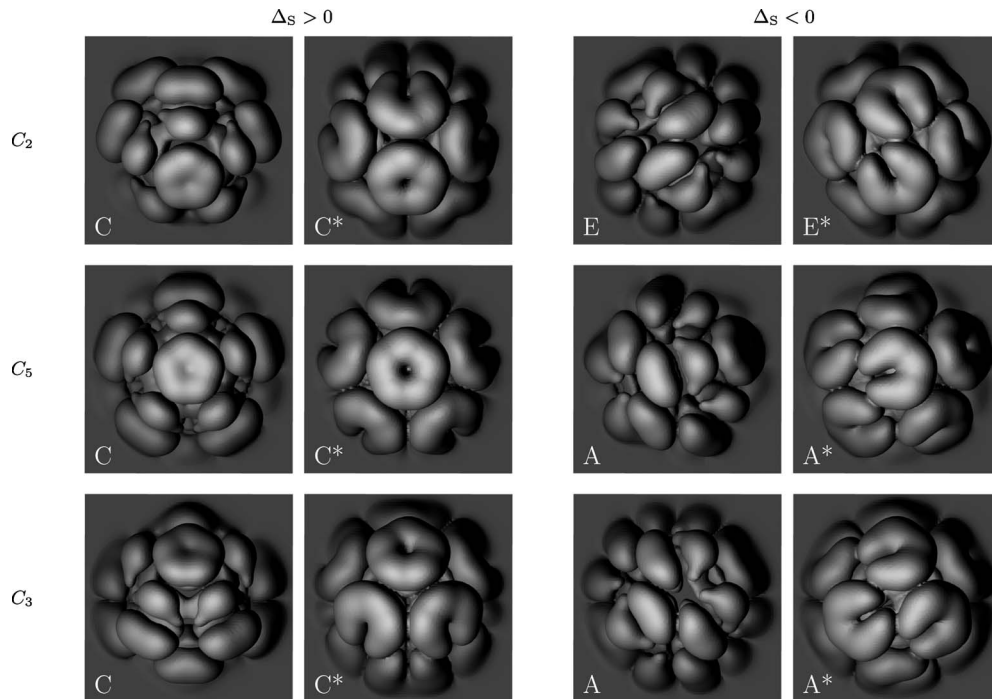

FIG. 5. High-resolution STM simulations of molecules locked into different D_{5d} wells. The absorption orientation is indicated by the axis label (C_2, etc.) which indicates which axis is normal to the surface, and an asterisk indicates the (degenerate) excited states.

of what the electronic distribution of the GS and ES (denoted by an asterisk) associated with a D_{5d} potential well appears like when the C_{60}^- ion is adsorbed in one of these geometries and then imaged by STM. The GS and ES images are complementary in the sense that summation of the two yields the usual picture of a set of degenerate T_{1u} LUMOs as shown in Fig. 2.

The images in a given column correspond to imaging the electronic distributions from different perspectives. The five-fold symmetry we would expect with a D_{5d} distortion is most obvious in the middle image of the two left-hand columns, which is where the molecule is observed along its associated C_5 axis with a pentagonal face pointing toward a surface. In the top and bottom images in those columns, the symmetric pentagon is rotated toward the bottom and top of the image, respectively, corresponding to the change in adsorption angle ϕ. The fivefold symmetry is not apparent in the two right-hand columns where different wells are favored, thus "disguising" the fact that the molecule is adsorbed in a pentagon-prone manner. This is because for the images associated with well E, the fivefold axis is oriented in the plane of the image from top left to bottom right. For well A, the fivefold axis is pointing slightly upward to the right of the image. Thus the absence of fivefold symmetry in observed images cannot be taken as an indication that the molecule does not have a fivefold distortion. The appearance of similar images but in different orientations for different molecules could be used to deduce the underlying symmetry. For example, a 72° ratcheting between five different images would be a sign that the molecule is being viewed along a C_5 axis of symmetry. However, a more realistic model of the surface interaction may remove the equivalence between different wells. A weak reduction in equivalence could result in all five orientomers being imaged, but some appearing more frequently than others, whereas a stronger interaction could result in some of the orientomers not featuring at all. Even here, however, the observation of a 72° angle, or a multiple thereof, between observed images would be a useful indicator of adsorption with a fivefold axis perpendicular to the surface and of the presence of a strong JT interaction.

B. D_{3d} distortion

For JT distortion to D_{3d} symmetry, there are ten orientomers that need to be considered. These correspond to the wells labeled a, b, ..., j in Table I and shown diagrammatically in Fig. 3(b). As before, we use the interaction with a simple planar surface to restrict our imaging to those wells most likely to undergo the largest energy changes when the isolated ion is adsorbed onto a surface. These energies are shown in Fig. 6, which indicates, for example, that if the D_{3d} ion is adsorbed with a hexagonal face prone to the surface, the ion is likely to either become locked into the well associated with that C_3 axis, or be equally likely to be in any one of six other equivalent wells. For the C_3 axis considered here, this means we only need to image well c and, say, well e (out of the equivalent set {a, b, e, f, h, j}). Again, this is consistent with Fig. 3(b).

Figure 7 shows the 12 most likely images expected for the GS and ES electronic distributions. Once again, the images
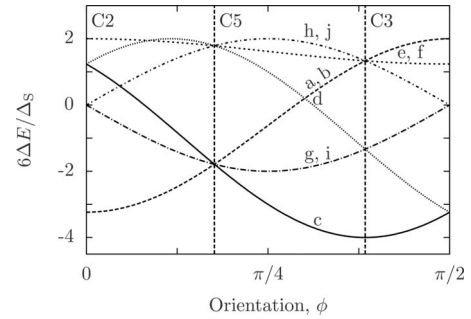

FIG. 6. The effect on the surface interaction energy for each D_{3d} well of varying the adsorption angle ϕ.

correspond to different views of just two distributions, viz., the unstarred GS distribution and the complementary starred ES distribution. In all but one of the 12 cases, symmetry equivalence is present and so observance of one orientomer would be accompanied by simultaneous observance of identical but differently oriented images. The unique case is that of a hexagon-prone ion (C_3 axis perpendicular to the surface) in which the surface stabilizes a single well, i.e., the two images on the bottom left-hand side of Fig. 7 corresponding to well c. This image is quite interesting because the GS electron density in the vicinity of the six uppermost carbon atoms forming the top hexagonal face is relatively small. (This is particularly apparent from a surface plot of the electronic density, see Fig. 24 of Ref. 23.) This would result in a fairly weak hexagonal appearance in a real STM trace with, perhaps, some likelihood that the three "triangular" lobes outside these atoms could feature in the image. On the other hand, the accompanying ES image is dominated by the three uppermost quasipentagonal lobes, which should produce a strong feature in an STM image which is very similar to that from a set of degenerate T_{1u} orbitals. That is, the resulting ES image would be similar to that produced from neutral C_{60}. Thus, it is possible that an image could be produced that would suggest C_{60}-like behavior which, in turn, would lead to the suggestion that the T_{1u} LUMOs are degenerate. Such a conclusion would be wrong as we are, by construction, dealing with a strongly distorted ion in which the JT effect has acted to (partly) remove the degeneracy. Apart from generating erroneous inferences, this would also mean that a strong JT effect had managed to elude observation under these circumstances.

C. D_{2h} distortion

For a JT distortion to D_{2h} symmetry there are 15 orientomers, corresponding to the 15 wells labeled $A, B, \ldots, O$ in Table I. The variation in the energy of these orientomers for different orientations with respect to our simple model surface is shown in Fig. 8. For this distortion type, there is the added complication that the degeneracy of the T_{1u} orbitals is completely removed. Thus, there is the possibility that two excited states could be separately imaged as well as the ground state. However, the excited states are degenerate in the limit when the two quadratic coupling parameters tend to zero. As quadratic coupling effects are expected to be smaller
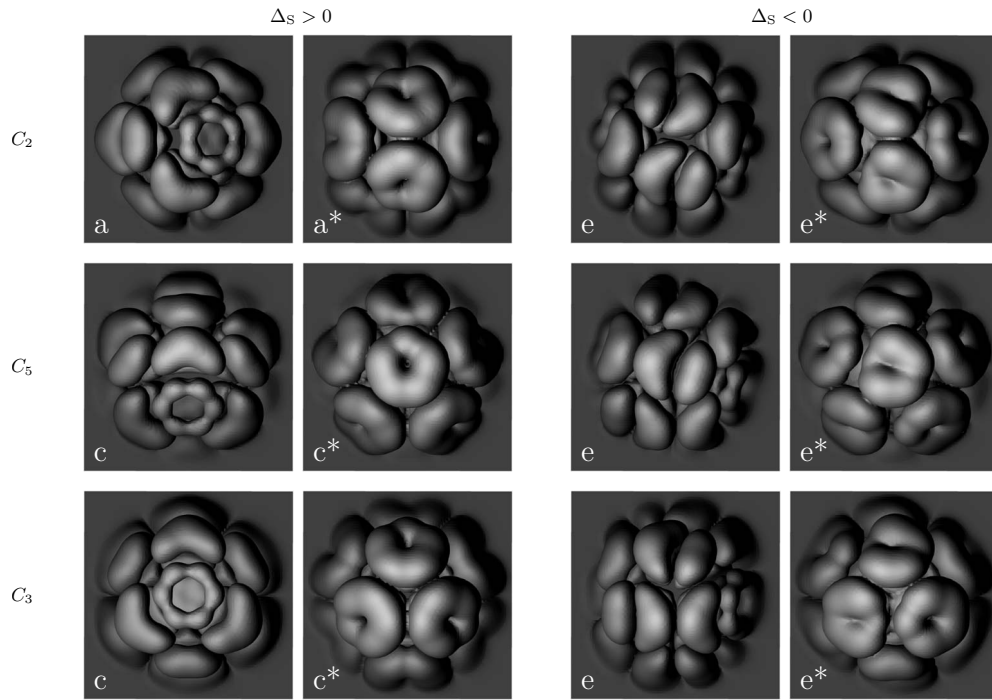
FIG. 7. High-resolution STM simulations of molecules locked into different D_{3d} wells. The absorption orientation is indicated by the axis label C2, etc., which is normal to the surface.

than linear effects, it may be that the separation between the excited states is too small for them to be imaged in isolation, that is, they may appear to be degenerate as far as STM measurements are concerned. To cover both of these eventualities, we image both excited states separately and in degenerate combination. The resulting images are collected in Fig. 9.

As well as the greater reduction in degeneracy, the D_{2h} case has other interesting features that distinguish it from the D_{5d} and D_{3d} ones. Disregarding the degenerate images, one sees that the three images expected for the same orientation but different sign of Δ_S are the same in each case except for their order. For example, for C2 orientation, the images corresponding to $\{A, A^*, A^{**}\}$ are identical to those from $\{N^*, N^{**}, N\}$. This suggests that if this case were to occur in practice, it is the relative order of the images with respect to the applied voltage that would give insight into the sign of Δ_S.

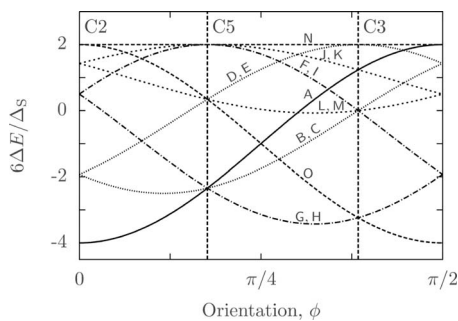There is another interesting facet to the case where the molecule has C2 orientation. For the simple surface interac-

tion assumed, the system could be locked into well A if $\Delta_S > 0$ or, if $\Delta_S < 0$, an equal mixture of wells N and O. Figure 9 shows the images expected for the $\{N, N^*, N^{**}\}$ states and Table I indicates that the equivalent set for well O is $\{O, O^*, O^{**}\} \equiv \{N^{**}, N, N^*\}$. Therefore, for instance, the other GS image expected to appear, in addition to that shown for well N, is the GS of well O which has the appearance of N^{**}. This image is completely different to that of well N. This is in contrast to the behavior of the other orientations/symmetries where equivalent sets of wells give the same image in each case but with each image having a different orientation with respect to rotation about the surface normal. Interestingly, although this behavior is only found in one particular distortion type and surface adsorption geometry, it is precisely these conditions that may be relevant in the STM images recorded by Wachowiak et al.,[6] as we will discuss in the next section.

D. Discussion

To summarize the current section, we have attempted to visualize via Figs. 5–9 the most likely ways in which a static JT effect might manifest itself in the C_{60}^- ion adsorbed on a surface. It is important to realize that the 18 scenarios covered by these images are likely to be mutually exclusive for a given surface. That is, we would expect that for a given surface we would find that the adsorbed C_{60} species would have some preferred adsorption orientation and unique JT distortion geometry. Similarly, the surface interaction, as defined, can only be positive or negative. However, even these 18 scenarios are not exhaustive as we have only considered three different absorption orientations and have used a rather simple surface interaction to determine to which groups of

FIG. 8. The effect on the surface interaction energy for each D_{2h} well of varying the adsorption angle ϕ.
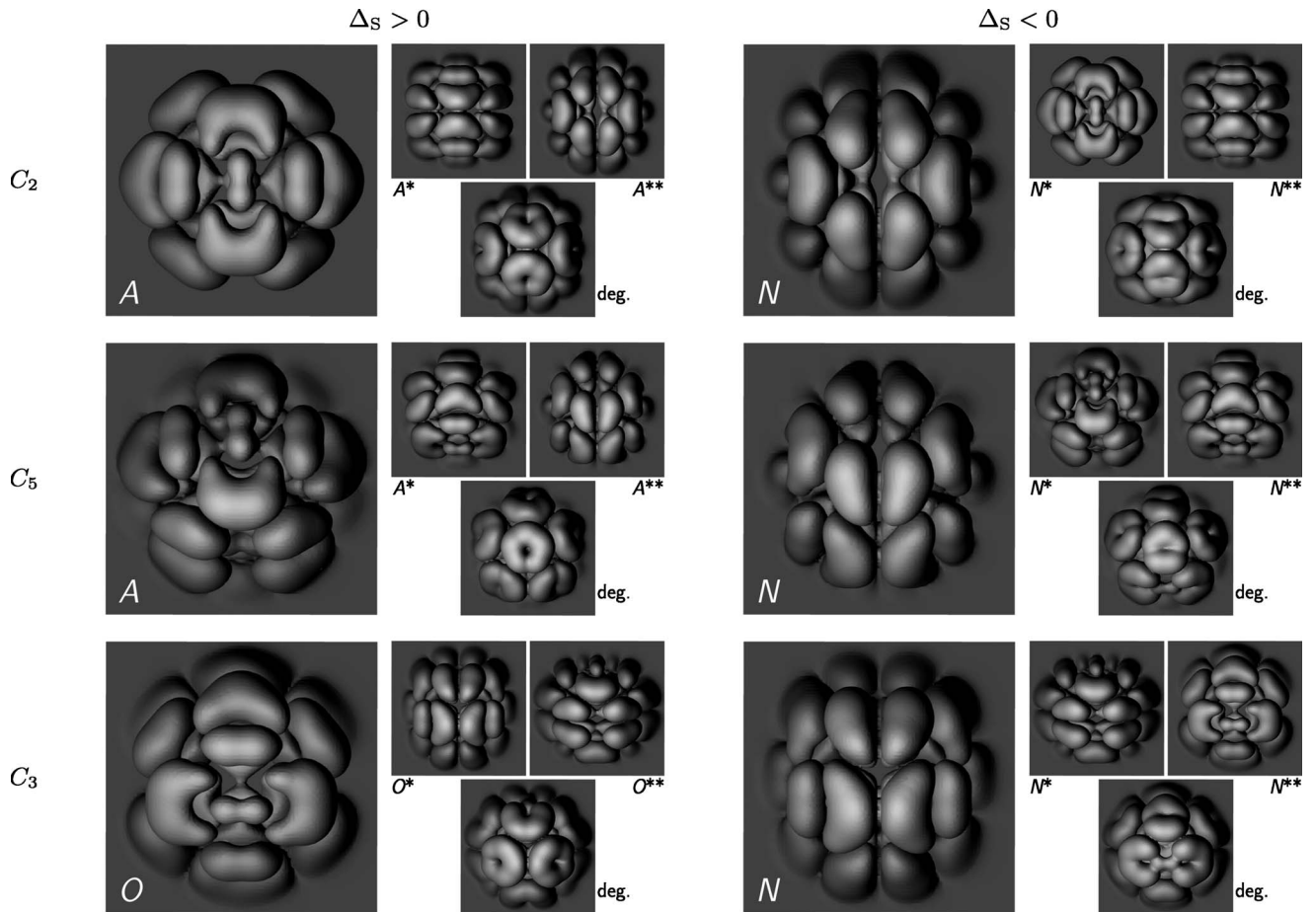
FIG. 9. High-resolution STM simulations of molecules locked into different D_{2h} wells. The absorption orientation is indicated by the axis label (C_2, etc.) which is normal to the surface. As the excited states are not generally degenerate, but may be close, images are drawn showing the states both on their own and when degenerate (labeled "deg."). Single and double asterisks indicate the states as ordered in Table I, e.g., $A^*=(1,0,0)$ and $A^{**}=(0,1,0)$.

orientomers are most likely to be favored. These shortcomings can be easily dealt with by generating further simulations to cover other absorption geometries and choice of orientomer. Extrapolation of their STM appearance to other views, not explicitly shown, may be made if required. Therefore, assuming the JT interaction is strong enough to engender a static distortion, we should be able to simulate the C_{60}^- ion's appearance via STM quite accurately provided we make the right choice of orientation and symmetry of JT distortion.

One final point worth remaking here is that the slow time scale associated with STM may mean that the intramolecular detail apparent in our STM simulations may not be visible because of dynamic effects. However, the unavoidable interactions with a host surface, or other neighbors, may have a dramatic effect on the ability of the C_{60} ions to enjoy this greater dynamic freedom. Coupled with the uncertainty over the strength of the JT effect in these ions, our images should still be highly relevant.

V. COMPARISON WITH EXPERIMENT

The images shown in Figs. 5, 7, and 9 indicate that a Jahn-Teller effect in the C_{60}^- ion that is sufficiently strong to lock the system into one particular distortion on an STM time scale would be capable of producing some very esoteric topographical motifs under favorable circumstances. We will now compare our images with real STM images found in the literature. We should first note that our images have been generated from the $T \otimes h$ JT interaction appropriate to C_{60}^- ions. Simulation of STM images from other C_{60}^{n-} species is a difficult task due to the complicated nature of JT effects in multicharged anions. However, one might expect images from other C_{60}^{n-} species to look rather similar. Also, CT upon adsorption onto different surfaces is not well quantified,[23] which means that it is not possible to unambiguously determine the charge state of a C_{60} molecule on a given surface. We will concentrate on situations in which the monoanion is thought to be prevalent, although we shall also consider other surfaces wherein the CT is thought to be different from unity, in the hope that agreement with our simulations may serve as evidence for the degree of charge actually transferred. Nevertheless, the above complications mean that an unequivocal identification of C_{60}^- ions is not possible at this stage.

The most popular surfaces used in STM studies of C_{60} adsorbates appear to be the noble metals, most notably gold and silver, although platinum has also been used. As these

surfaces are inert, the expectation is that the C_{60} molecules adsorbed onto them will retain their integrity. As far as CT is concerned, it is thought that only one or two electrons may be transferred to the cage molecule upon adsorption, with the actual degree of transfer depending on the crystal face presented to the adsorbate. Thus, there is a high expectation that the C_{60}^{-} anion could be present on these surfaces.

Comparison with experimental data is not a trivial task. A comparison can only be made if the STM data is sufficiently resolved. The experiment must also be conducted at a low temperature to avoid loss of intramolecular detail due to molecular rotation on the surface. Even under these conditions it is plausible that similar surface-C_{60} systems could produce different images if their method of production is not identical. For example, STM samples are often annealed before imaging. The thermal jostling of the adsorbed molecules usually produces more uniform images but there is also the possibility that other changes could be induced by the annealing process such as a change in charge state.

Clearly, an isolated anion must have a unique preferred distortion geometry corresponding to which distortion produces the lowest energy. The difference in energy between D_{5d}, D_{3d}, and D_{2h} distortions, however, could be very small as these differences depend on second-order vibronic coupling constants, the magnitudes of which are unknown but are expected to be small. Therefore, under the influence of a surface interaction, it is quite feasible that any of these distortions could be preferred. The complexity of the problem is further exacerbated by the roughly spherical geometry of the C_{60} cage which means that the molecule also has a degree of rotational freedom in which to orient itself to find the absorption orientation of lowest energy. Thus, we will try to cover a wide range of possible outcomes. In any particular experiment the actual behavior will depend on many factors and we shall not attempt to make firm predictions for particular surfaces. Instead, we shall attempt to make an analysis of the available experimental data to search for agreement with our predicted images in order to make deductions about the system imaged.

As our theory has treated the surface interaction as of secondary importance to the JT interaction, we will begin our comparison with experimental data by considering results in which an organic buffer layer has been used as an intermediary between C_{60} molecules and a metal substrate in an attempt to reduce the interaction between the C_{60} molecules and surface. We will then consider Au, Ag, and Si surfaces, where surface interactions play a more dominant role and our assumption that the surface interactions can be treated as a perturbation with respect to JT interactions may not be appropriate.

A. Surfaces with buffer layers

Franke *et al.*[26] were able to produce good images of C_{60} adsorbed onto a tetraphenyladamantane (TPA)/Au(111) support consistent with all molecules having the same orientation (hexagon prone) and with LUMOs that retain their degeneracy, which is indicative of a neutral molecule with no JT distortion. However, not all results for C_{60} molecules on a
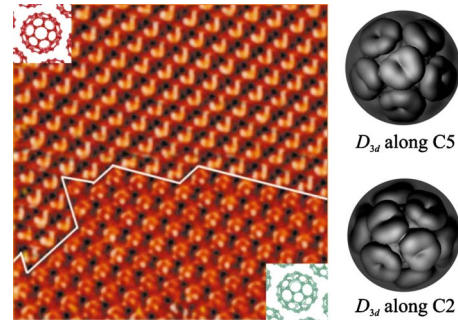

FIG. 10. (Color online) Experimental STM images of C_{60} molecules on an alkylthiol SAM on Au(111), reprinted from part of Fig. 2 of Ref. 27 with permission from Macmillan Publishers Ltd, Copyright (2001). The insets show their suggested molecular orientations. To the right are possible matches taken from our STM simulations of JT-distorted C_{60}^{-} ions.

buffer layer can be interpreted in this manner. Some particularly interesting images were obtained by Hou *et al.*[27] and Yuan *et al.*[28] using an alkylthiol self-assembled monolayer (SAM) on a gold support. In these two separate works on similar SAMs, ostensibly different images were obtained as shown in Figs. 10 and 11.

In Fig. 10, the experimental image indicates long-range order in the electronic structure of the adsorbed C_{60} units. Two domains are evident, which are believed to correspond to two different orientations of the molecules. However, the suggested orientation for the upper domain in Fig. 10, viz., hexagon prone (shown inset), would be expected to show threefold symmetry, which does not tally with the STM image which appears "v" shape. A very good match to the observed image is found in image e* of the $\Delta_S < 0$ case in Fig. 7, which arises from a C_{60}^{-} ion adsorbed with a pentagon prone to the surface and subject to a D_{3d} JT distortion. A v shape is produced because, in this arrangement, a node appears at one of the atoms of the uppermost pentagon. A match to the other domain can also be obtained from a D_{3d} distorted ion assuming the ion is adsorbed with a double bond prone to the surface (Fig. 7, image e*, $\Delta_S < 0$). The
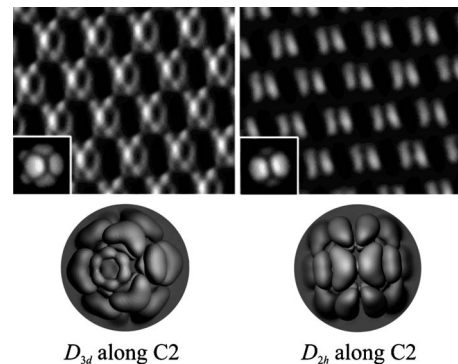

FIG. 11. Experimental STM images of C_{60} molecules on an alkylthiol SAM on Au(111), reprinted from Fig. 1 of Ref. 28 with permission from American Chemical Society, Copyright (2003). The authors' simulations are shown inset into each image. Below are possible matches taken from our STM simulations of JT-distorted C_{60}^{-} ions.

experimental images therefore appear to be better explained by our model involving a JT effect than the non-JT explanation of the authors.

Seemingly different images of C_{60} on alkylthiol SAM were obtained by Yuan *et al.*,[28] as shown in Fig. 11. Once again, two domains appear to prevail. The authors' own simulations that were provided to explain the observed data are shown inset in each figure. It is interesting that the features in the actual STM images appear to be much narrower than in the simulations. As this is the same surface as that used by Hou *et al.*,[27] comparison with the D_{3d}-derived images in Fig. 7 should be our first resort. Indeed, as shown in Fig. 11, a good match to one of the STM images (the left-hand side) can be found assuming that a D_{3d}-distorted molecule is adsorbed with C_2 axis normal to the surface. Some justification of this match is required. With smaller tunneling currents, the uppermost two atoms will become more prominent as they are closer to the STM tip, producing the bright feature in the C_{60} motif. The four nearest neighbors to these uppermost atoms can be seen to be ideally placed to match with surrounding features in the STM image, leaving a hexagonal "cavity" to the right formed with two further-away atoms that would be normally weak but feature because they happen to host a high electron density.

Interestingly, nothing of D_{3d} origin appears to match the right-hand image in Fig. 11, forcing us to seek a match with ions having a different distortion. We note that each individual C_{60} appears to be exhibiting twofold rotational symmetry, consistent with adsorption with a double bond prone to the surface. A possible match, as shown in Fig. 11, can be achieved if we assume the ion undergoes D_{2h} distortion. As can be seen, this match would be expected to be superior to the original authors' simulation (shown inset) because the pentagonal lobes responsible for their image have an additional node inside them in the D_{2h} orbital shown. This makes the STM image narrower, as observed. However, it is noted that the proposed D_{2h} match actually corresponds to an excited state orbital and one must question whether such an orbital could be imaged at the same bias as the D_{3d} ground state one shown next to it.

It is indeed interesting that different JT distortions appear to fit the images observed in Fig. 11. Ordinarily and intuitively, one would expect there to be one preferred distortion corresponding to the JT distortion which produces the greatest energy gain. However, the differences in JT energy arising from D_{3d}, D_{2h}, or D_{5d} distortion only depends on quadratic coupling so could be quite small. The situation is similar to absorption of C_{60} on a surface; one would expect a particular orientation to occur exclusively corresponding to the orientation having the largest adsorption energy. Nevertheless, it is clear that domains of differently oriented molecules can be sustained on the same surface due to additional stabilizing factors, e.g., intermolecular interactions, competing adsorption sites, etc. Therefore, there is no reason why differently distorted molecules may not coexist on the same surface and be stabilized by different absorption orientations and sites, intermolecular interactions (e.g., cooperative JT effects), etc. This is something that may become apparent in future STM studies.
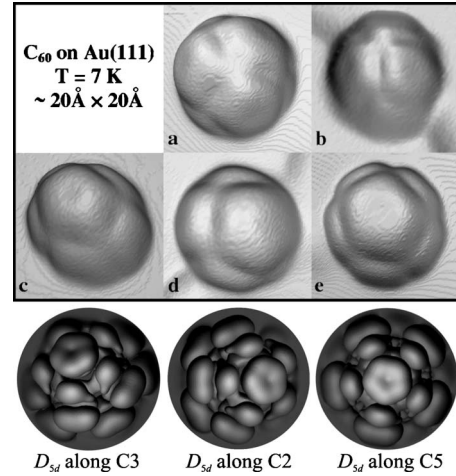

FIG. 12. STM images of C_{60} molecules on Au(111), reproduced from Ref. 31. The images were observed at a sample bias of 2 V with relative abundances (a) 38%, (b) 35%, (c) 13%, (d) 8%, and (e) 6%. The latter three images are very similar to those expected from differently oriented D_{5d}-distorted anions, as shown along the bottom of the figure.

B. Au surfaces

For this substrate, there is evidence that one electron per C_{60} is transferred from the surface upon adsorption,[29,30] making it an ideal candidate for observations of the JT-influenced STM images as long as the surface interactions are not so strong that they dominate JT interactions. However, other studies, for example, the DFT calculations of Lu *et al.*,[31] suggest that CT is negligible on Au(111). In this latter work, the authors also present low-temperature (7 K), high-resolution STM images of individual C_{60} adsorbates on Au(111).

Lu *et al.*'s images, reproduced in Fig. 12, can be most readily explained by assuming that the C_{60} molecules are adsorbed onto the gold surface with a variety of different orientations. We note that the STM images were recorded using a bias of 2 V, which indicates that the orbitals responsible for the images are the T_{1g} LUMO+1 orbitals. However, the set of degenerate LUMO+1 orbitals has the same appearance as a set of degenerate T_{1u} LUMOs.[5] The images in Fig. 12 therefore suggest that the LUMO+1 orbitals are degenerate as far as the STM apparatus is concerned. Any loss of degeneracy due to surface or JT effects must, therefore, be small.

Although Lu *et al.*'s images can be adequately explained using orientation arguments, it is still worth examining them to see if an alternative explanation in terms of the JT effect can be formulated. Fivefold symmetric features in the observed electronic distributions are apparent. Therefore, if a JT effect is present, a distortion to D_{5d} symmetry is suggested. Indeed, three of the simulated images (Fig. 5, first column) bear a strong resemblance to three of those in Fig. 12. To reinforce this resemblance, we have included the relevant images underneath their STM counterparts in Fig. 12, where our images have been rotated to emphasize the correspondence. However, we also need to account for the other

two images (a and b in Fig. 12), which actually have the dominant presence (73%) on the surface. This cannot be done using D_{5d}-distorted ions. Threefold and twofold symmetric images could be formed if we assume that D_{3d}-distorted ions can coexist on the surface. Even considering surface inhomogeneity, this seems very unlikely. Another possible explanation is that the final two images could arise from neutral molecules rather than anions. In this case, the image in Fig. 12 labeled a (threefold symmetry) would be the neutral counterpart to the image labeled c, with a similar correspondence between images b (twofold symmetry) and d. Comparing these images, one sees that the additional charge on the C_{60} would then have the effect of "pushing out" one of the upper lobes of the molecular orbital. In this respect, the image labeled e in Fig. 12 would be the same for both C_{60}^0 and C_{60}^-.

A distribution of monoanions and neutral molecules on the surface is not inconceivable and, in fact, would be expected if the average CT upon adsorption is <1. Assuming that image a (38%) and image c (13%) gives the relative numbers of neutral versus singly charged species, we calculate an average CT of 0.25 e/C_{60}. However, the DFT calculations of Lu et al.,[31] we recall, suggest that the CT is negligible. Clearly, if the actual CT can be determined more accurately on this surface then the validity of the alternative JT-based explanation given here for the images in Fig. 12 can be tested. We readily admit, however, that the simpler explanation using orientation arguments alone seems the most likely one to be correct. Indeed, strong support for this interpretation is demonstrated by the observation[32] of a C_{60} (7 $\times$ 7) superstructure in a C_{60} monolayer on Au(111) in which orientation appears to show long range order. On the other hand, Frederiksen et al.[33] have taken very interesting tunneling spectra from C_{60} molecules adsorbed into the troughs formed between rows of 1,3,5,7-TPA molecules adsorbed onto a Au(111) surface. Their high-resolution spectra recorded from these "suspended" C_{60} molecules show a vibronic side band to the main LUMO resonance which they successfully modeled using DFT calculations and assuming a dynamic JT effect. The decoupling from the metallic surface was thought to be sufficient to allow the subtle JT effect to be apparent. However, a JT effect would only be present if the C_{60} molecules were charged and so this evidence suggests that the studied species were in fact charged. We would not expect the hydrocarbon TPA to participate in electron donation and so significant CT from Au(111) to the C_{60} is suggested. Unfortunately, the STM images in Ref. 33 are insufficiently spatially resolved to facilitate comparison with the STM simulations made here.

Another interesting paper on the C_{60}-Au(111) system was recently published by Červenka et al.[34] These authors used a different technique to produce their C_{60} adlayers, namely, spray deposition. One of their STM images, recorded at a bias of 2.5 V, is reproduced in Fig. 13. The individual molecular motifs clearly appear cooperatively aligned and closely resemble one of the JT-induced images (D_{5d} distortion with a C_2 directed to the surface). Surprisingly, there is no mention of the other types of image recorded by Lu et al. (Fig. 12). It may be that this orientation is favored by the additional interaction with its neighbors, causing mutual
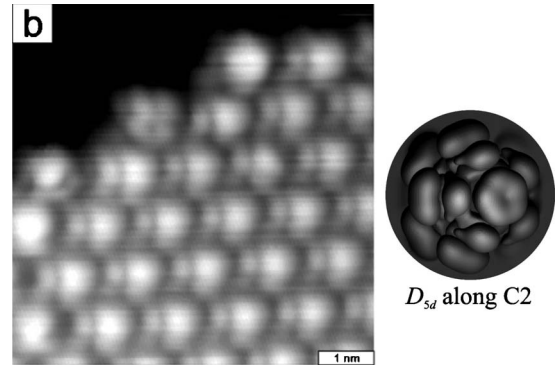

FIG. 13. High-resolution STM image of a spray deposited C_{60} monolayer on Au(111), reprinted from part of Fig. 3 of Ref. 34 with permission from the Institute of Physics. The experimental image was recorded at 5 K using a sample bias of 2.5 V. The individual molecular images are very similar to those expected from a D_{5d}-distorted anion adsorbed with a C_2 axis prone to the surface, as shown on the right of the figure.

alignment. However, if the JT effect is playing a rôle in determining the intramolecular detail observed, then a cooperative (intermolecular) JT effect could be influencing the long-range order apparent in Fig. 13.

Finally, although not entirely appropriate because of an expected high charge state, we briefly discuss the work carried out by Crommie and co-workers on doped C_{60}-Au systems.[6,35,36] In these works, the authors codeposit potassium metal onto the gold surface with the C_{60} molecules in order to facilitate CT to the fullerene. Depending on the doping levels, several phases with a general formula K_xC_{60} have been imaged. Wachowiak et al.[6] presents evidence for a static JT effect in a layer with nominal formula K_4C_{60}. We reproduce the STM images of the K_4C_{60} phase recorded using tunneling biases slightly above and below (± 0.1 V) the Fermi energy in Fig. 14. The authors' logic appears to be that if there were no JT effect, then the T_{1u} orbitals would all be degenerate so that the images expected at ± 0.1 V bias would be identical. Indeed, this principle is used to deduce an absence of a JT effect in another phase of nominal formula K_3C_{60}. However, it is clear that the interaction of the C_{60} units with the surface and among themselves also needs to be taken into account at the same time. In Fig. 14, we show STM simulations of a set of T_{1u} orbitals assuming that each component is sufficiently separated in energy from the other components so that they may be separately imaged. If these orbitals are arranged in the order $z < x < y$ in terms of increasing energy, and then filled with four electrons in the usual manner, then the observed experimental STM images with respect to the Fermi energy can be readily explained.

The reason that the orbitals should be so ordered, energy-wise, could be simply down to the degree each orbital interacts with the surface. However, it is noteworthy that the HMO simulations shown in Fig. 14 (bottom) are exactly the same as those shown in Fig. 9 for a D_{2h}-distorted JT effect with $\Delta_S > 0$ and C2 as the absorption orientation. This is not surprising as this type of JT distortion completely removes the degeneracy of the T_{1u} orbitals and therefore, may be one mechanism for the degeneracy loss required, but by no
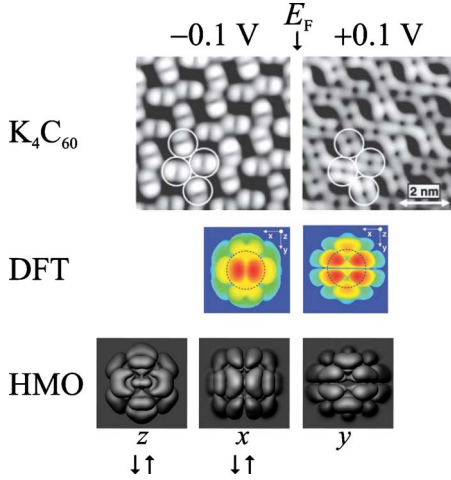
FIG. 14. (Color online) (Top) Experimental STM images of a nominally K_4C_{60} monolayer on Au(111) recorded at biases slightly above and below the Fermi energy (E_F; $T=7$ K), and (middle) DFT simulations of a D_{2h}-distorted C_{60}^{4-} ion, reprinted from parts of Figs. 3 and 4 of Ref. 6 with permission from AAAS. (Bottom) Our STM simulations of a set of nondegenerate T_{1u} orbitals, where $x \equiv T_{1ux}$, etc. At the very bottom, the arrows represent HMO occupancy and all simulations assume a C_2 axis is normal to the surface.

means the only mechanism. It is also interesting that DFT simulations made by Wachowiak et al.,[6] and also shown in Fig. 14 (middle), are very similar to our HMO simulations. In fact, the DFT simulation for the filled states would be even more closely reproduced if the T_{1uz} and T_{1ux} orbitals were quasidegenerate, a situation that might be expected to occur if these orbitals were being driven by energy considerations to achieve their lowest possible energies at the expense of the unfilled orbital. Overall, therefore, it seems that the STM images in Fig. 14 cannot be interpreted as unequivocal evidence for the JT effect in this system.

C. Ag surfaces

Silver has a smaller work function than gold and so the charge transfer to adsorbed C_{60} molecules is expected to be greater. In fact, estimates for the CT vary from 0.75 to 1 electron per C_{60} molecule, depending on the crystal surface utilized.[30,37,38] Several high-resolution STM studies of interest can be found in the literature.[39–42] Those which concentrate on the observation that individual C_{60} molecules tend to fall into two distinct categories on this surface, each category possessing different apparent heights or brightnesses and usually referred to as the bright-dim (BD) contrast. Apart from brightness, the distinct sets of molecules also seem to have different orientations. Figure 15 reproduces a typical STM image[39] on Ag(100) which clearly shows the BD contrast and apparent orientation differences between the two types of molecule. The precise explanation for the orientational differences does not seem to be fully established yet, although surface reconstruction has been shown to be a likely candidate.[43]

From a JT point of view, should the BD contrast relate to ions possessing different charge states, then the bright and
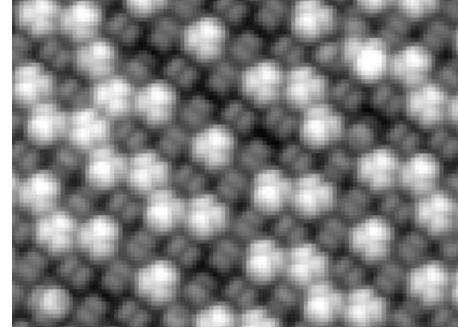

FIG. 15. STM image of a C_{60} monolayer on Ag(001) adapted from Ref. 39. The tunneling parameters used were 2 V bias and 1 nA tunneling current ($T=7$ K). The BD contrast is clearly visible.

dim species would be expected to have different intramolecular JT interactions and, therefore, appearance. Furthermore, at least one of the species would require a JT treatment different to the one given here. This notwithstanding, the high-resolution images constitute valuable information that should be considered here.

It is easy to see that the dim species have apparent twofold symmetry and a comparison with Figs. 5, 7, and 9 allows one to find a match with this double-lobed image for each of the JT distortions shown (D_{5d}, D_{3d}, and D_{2h}). Similarly, the bright species have slightly off-axis threefold symmetry which resemble several of our STM simulations but are not sufficiently idiosyncratic enough to distinguish them from the non-JT interpretations made by the original authors themselves. It thus seems that none of the images collected on silver to date provide any evidence for a static JT effect of the type considered here.

D. Si surfaces

Some very detailed STM images have been captured of C_{60} adsorbed on a Si(111)-(7×7) surface.[44,45] In particular, Pascual et al.[45] observed a series of interesting images at a variety of biases ranging from −2 to +2 V, all of which appeared to match molecular orbitals derived from C_{60}'s HOMOs. In Fig. 16, we reproduce one of their experimental STM images (labeled "c") which was recorded at a bias of 2 V. The authors found that their image closely resembled that obtained from their DFT calculations involving a doubly degenerate pair of HOMO-derived orbitals (image "g" in Fig. 16). We also found similar agreement with our HOMO-derived orbital obtained using HMO theory.[5] However, Pascual et al.[46] themselves acknowledge that one would not expect to find a HOMO-derived orbital at a bias of 2 V, so we will explore if an alternative JT-based explanation is possible.

Using our results, we can see that there is a way in which a similar image can be derived from the T_{1u} LUMOs if there is a JT effect which favors D_{5d} distortion. Figure 16 shows two simulated images for a D_{5d}-distorted C_{60}^- anion viewed along the corresponding C_5 axis (Fig. 5 with $\Delta_S > 0$) rotated to match the other images. The upper image shows results that could be expected from a HR STM experiment, and the lower image shows a lower resolution (LR) result that could
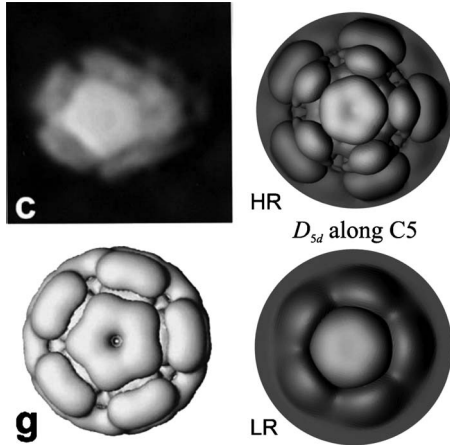
FIG. 16. The two left-hand images are reprinted from parts of Fig. 2 of Ref. 45 with permission from Elsevir, Copyright (2000). Uppermost is an experimental STM image of a C_{60} molecule adsorbed onto Si(111)-(7×7) and below that is a HOMO-derived orbital calculated using local-density approximation-DFT. The labels c and g are retained from the original work. The two right-hand images are our LUMO-derived STM simulations of a D_{5d}-distorted C_{60} anion adsorbed with a pentagonal face prone to the surface. The upper image simulates a high-resolution STM image and the lower image simulates the image that would be obtained with a 22-fold reduction in current.

be obtained with a 22-fold reduction in current. In the HR simulation, the central pentagon appears to be in the wrong orientation. However, in the LR simulation, the tip has responded to the more diffuse outer parts of the orbital to fill in the spaces near the surrounding nodes. This changes the central pentagon to match the results of Pascual *et al.* This effect was highlighted in Fig. 5 of Ref. 5. Thus it is possible that the images captured by Pascual *et al.*[45] could, in fact, be providing evidence for a static JT effect in this system. In this respect, it is interesting that a distortion to D_{5d} symmetry is once again suggested.

VI. CONCLUSIONS

Our simulations shown in Figs. 5, 7, and 9 cover many different possible scenarios that may occur should a strongly JT-distorted C_{60}^- ion adsorbed onto a surface be imaged using STM. Of course, if the JT effect is not particularly strong then the image expected would be the same as that obtained from a set of degenerate LUMOs. However, if it is strong, then some very characteristic images could be expected to be observed under the right conditions. We have endeavored to discuss all STM images here that have appeared in the literature that are sufficiently highly resolved for a comparison to be made. Several good matches have been found, which could indicate that the species involved were, in fact, JT-distorted C_{60}^- ions. However, none of our simulations give a significantly better interpretation of the data sets considered compared to alternative non-JT interpretations. One reason for this could be that the individual C_{60} molecules are still not sufficiently resolved in STM experiments in order to discern the distortions we predict. Another possibility is that the
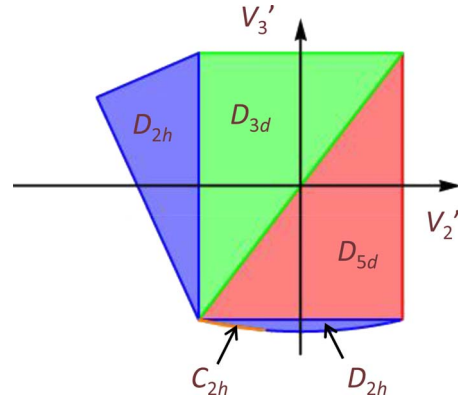

FIG. 17. (Color online) Regions of D_{5d}, D_{3d}, and D_{2h} symmetries for the $T \otimes h$ JT problem.

JT effects we are trying to identify are too small in the systems imaged so far, or are too highly quenched on surfaces to be observed.

Hopefully, further STM experiments with increased resolution or using yet untried surfaces may yield images that cannot be explained using traditional methods employing non-JT theories. Thus, our hope is that the images we have provided here may serve as reference images that can be used to identify particular JT interactions in such circumstances.

Finally, another complication to bear in mind is that the JT effect, even if present, is actually a dynamic interaction (depending on time scale) and this will also have an effect on the images recorded. This is an issue we intend to return to in a subsequent work.

APPENDIX

Reference 24 calculated the positions of wells in the lowest APES of the $T_{1u} \otimes h_g$ JT problem of D_{5d}, D_{3d}, and D_{2h} symmetries, along with their corresponding energies

$$E_{D_{5d}} = -\frac{1}{5 - 4\sqrt{2}V_2'}\frac{V_1^2}{\mu\omega^2},$$

$$E_{D_{3d}} = -\frac{1}{5 - 4\sqrt{10}V_3'/3}\frac{V_1^2}{\mu\omega^2},$$

$$E_{D_{2h}} = -\frac{1 + V_2'/4\sqrt{2} + 9V_3'/4\sqrt{10}}{5 - V_2'^2 - 3V_3'^2}\frac{V_1^2}{\mu\omega^2}, \tag{A1}$$

respectively, where V_1 is the linear coupling constant, $V_2' = V_2/\mu\omega^2$ and $V_3' = V_3/\mu\omega^2$ are dimensionless quadratic coupling constants, μ is the mass, and ω the frequency of the h_g mode. It was concluded that the D_{2h} points can never be absolute minima. However, this was assuming that the qua-

dratic coupling constants must be positive. Whilst negative quadratic coupling constants will not lower the energy as much as with just linear or linear and positive quadratic couplings, the energy is still lowered compared to the non-JT case. Hence the possibility of negative quadratic coupling constants cannot be ruled out.

When negative couplings are considered, it is found that there are regions of strong quadratic coupling for which the D_{2h} points can be absolute minima, as well as a very small region of C_{2h} minima. This is shown in Fig. 17. For the system to be stable, the conditions $V_2' < 5/4\sqrt{2}$, $V_3' < 3\sqrt{5}/4\sqrt{2}$, $V_3' > -\sqrt{10} - \sqrt{5}V_2'$, $V_3' < V_2'/\sqrt{5} + \sqrt{5/2}$, and $V_2'^2$

$+ 3V_3'^2 < 5$ must be obeyed. These conditions form the boundaries of the regions in Fig. 17. Outside these ranges, the minimum energy is unbounded and so the system is unstable. (Note that Ref. 24 only looked for turning points in the energy and did not consider unbounded solutions.) The boundary between the D_{5d} and D_{3d} regions is given by $3V_2' = \sqrt{5}V_3'$. It is not possible to find an analytical expression for the boundary between the D_{2h} and C_{2h} regions but numerically it is found to be midway between the lines defined by the elliptical boundary $V_2'^2 + 3V_3'^2 = 5$ and the line $V_3' = [-5\sqrt{2} - \sqrt{10} + (1 - \sqrt{5})V_2']/(1 + 3\sqrt{5})$.

---

*janette.dunn@nottingham.ac.uk;   http://www.nottingham.ac.uk/~ppzjld

[1] G. Binnig and H. Rohrer, Helv. Phys. Acta **55**, 726 (1982).

[2] G. Binnig and H. Rohrer, IBM J. Res. Dev. **30**, 355 (1986); **44**, 279 (2000).

[3] C. Bai, *Scanning Tunneling Microscopy and Its Application*, 2nd ed. (Springer, New York, 2000).

[4] C. J. Chen, *Introduction to Scanning Tunneling Microscopy*, 2nd ed. (Oxford University Press, New York, 2008).

[5] I. D. Hands, J. L. Dunn, and C. A. Bates, Phys. Rev. B **81**, 205440 (2010).

[6] A. Wachowiak, R. Yamachika, K. H. Khoo, Y. Wang, M. Grobis, D. H. Lee, S. G. Louie, and M. F. Crommie, Science **310**, 468 (2005). Parts of Figs. 3 and 4 reprinted with permission from AAAS.

[7] A. F. Hebard, M. J. Rosseinsky, R. C. Haddon, D. W. Murphy, S. H. Glarum, T. T. M. Palstra, A. P. Ramirez, and A. R. Kortan, Nature (London) **350**, 600 (1991).

[8] M. J. Rosseinsky, A. P. Ramirez, S. H. Glarum, D. W. Murphy, R. C. Haddon, A. F. Hebard, T. T. M. Palstra, A. R. Kortan, S. M. Zahurak, and A. V. Makhija, Phys. Rev. Lett. **66**, 2830 (1991).

[9] O. Gunnarsson, Rev. Mod. Phys. **69**, 575 (1997).

[10] M. C. M. O'Brien, J. Phys. C **16**, 85 (1983).

[11] F. Besenbacher, E. Lægsgaard, and I. Stensgaard, Mater. Today **8**, 26 (2005).

[12] C. C. Chancey and M. C. M. O'Brien, *The Jahn-Teller Effect in C_{60} and other Icosahedral Complexes* (Princeton University Press, Princeton, 1997).

[13] I. D. Hands, J. L. Dunn, and C. A. Bates, Phys. Rev. B **73**, 014303 (2006).

[14] I. D. Hands, J. L. Dunn, and C. A. Bates, Phys. Rev. B **73**, 235425 (2006).

[15] I. D. Hands, L. M. Sindi, J. L. Dunn, and C. A. Bates, Phys. Rev. B **74**, 115410 (2006).

[16] O. Gunnarsson, H. Handschuh, P. S. Bechthold, B. Kessler, G. Ganteför, and W. Eberhardt, Phys. Rev. Lett. **74**, 1875 (1995).

[17] I. D. Hands, J. L. Dunn, and C. A. Bates, Phys. Rev. B **63**, 245414 (2001).

[18] C. M. Varma, J. Zaanen, and K. Raghavachari, Science **254**, 989 (1991).

[19] I. D. Hands, J. L. Dunn, and C. A. Bates, in *Vibronic Interactions: Jahn-Teller Effect in Crystals and Molecules*, NATO Sci-

ence Series Vol. 39, edited by M. D. Kaplan and G. O. Zimmerman (Kluwer Academic, Dordrecht, 2001), pp. 285–289.

[20] V. P. Antropov, O. Gunnarsson, and A. I. Liechtenstein, Phys. Rev. B **48**, 7651 (1993).

[21] N. Manini, A. Dal Corso, M. Fabrizio, and E. Tosatti, Philos. Mag. B **81**, 793 (2001).

[22] M. Saito, Phys. Rev. B **65**, 220508 (2002).

[23] I. D. Hands, J. L. Dunn, C. S. A. Rawlinson, and C. A. Bates, in *The Jahn-Teller Effect*, Springer Series in Chemical Physics Vol. 97, edited by H. Koeppel, D. R. Yarkony, and H. Barentzen (Springer-Verlag, Berlin, 2009), pp. 517–551.

[24] J. L. Dunn and C. A. Bates, Phys. Rev. B **52**, 5996 (1995).

[25] I. D. Hands, W. A. Diery, C. A. Bates, and J. L. Dunn, Phys. Rev. B **76**, 085426 (2007).

[26] K. J. Franke, G. Schulze, N. Henningsen, I. Fernández-Torrente, J. I. Pascual, S. Zarwell, K. Rück-Braun, M. Cobian, and N. Lorente, Phys. Rev. Lett. **100**, 036807 (2008).

[27] J. G. Hou, J. L. Yang, H. Q. Wang, Q. X. Li, C. G. Zeng, L. F. Yuan, B. Wang, D. M. Chen, and Q. S. Zhu, Nature (London) **409**, 304 (2001). Part of Fig. 2 reprinted with permission from Macmillan Publishers Ltd, Copyright (2001).

[28] L.-F. Yuan, J. Yang, H. Wang, C. Zeng, Q. Li, B. Wang, J. G. Hou, Q. Zhu, and D. M. Chen, J. Am. Chem. Soc. **125**, 169 (2003). Figure 1 reprinted with permission from the American Chemical Society, Copyright (2003).

[29] S. Modesti, S. Cerasari, and P. Rudolf, Phys. Rev. Lett. **71**, 2469 (1993).

[30] B. W. Hoogenboom, R. Hesper, L. H. Tjeng, and G. A. Sawatzky, Phys. Rev. B **57**, 11939 (1998).

[31] X. Lu, M. Grobis, K. H. Khoo, S. G. Louie, and M. F. Crommie, Phys. Rev. B **70**, 115418 (2004).

[32] G. Schull and R. Berndt, Phys. Rev. Lett. **99**, 226105 (2007).

[33] T. Frederiksen, K. J. Franke, A. Arnau, G. Schulze, J. I. Pascual, and N. Lorente, Phys. Rev. B **78**, 233401 (2008).

[34] J. Červenka and C. F. J. Flipse, Nanotechnology **21**, 065302 (2010). Part of Fig. 3 reprinted with permission from Institute of Physics.

[35] Y. Wang, R. Yamachika, A. Wachowiak, M. Grobis, K. H. Khoo, D. H. Lee, S. G. Louie, and M. F. Crommie, Phys. Rev. Lett. **99**, 086402 (2007).

[36] Y. Wang, R. Yamachika, A. Wachowiak, M. Grobis, and M. F. Crommie, Nature Mater. **7**, 194 (2008).

[37] L. H. Tjeng, R. Hesper, A. C. L. Heessels, A. Heeres, H. T.

Jonkman, and G. A. Sawatzky, Solid State Commun. **103**, 31 (1997).

[38] C. Cepek, M. Sancrotti, T. Greber, and J. Osterwalder, Surf. Sci. **454**, 467 (2000).

[39] M. Grobis, X. Lu, and M. F. Crommie, Phys. Rev. B **66**, 161408(R) (2002).

[40] X. Lu, M. Grobis, K. H. Khoo, S. G. Louie, and M. F. Crommie, Phys. Rev. Lett. **90**, 096802 (2003).

[41] X. Zhang, W. He, A. Zhao, H. Li, L. Chen, W. W. Pai, J. Hou, M. M. T. Loy, J. Yang, and X. Xiao, Phys. Rev. B **75**, 235444 (2007).

[42] M. Grobis, R. Yamachika, A. Wachowiak, X. Lu, and M. F. Crommie, Phys. Rev. B **80**, 073410 (2009).

[43] C.-L. Hsu and W. W. Pai, Phys. Rev. B **68**, 245414 (2003).

[44] J. G. Hou, Jinlong Yang, Haiqian Wang, Qunxiang Li, Changgan Zeng, Hai Lin, Wang Bing, D. M. Chen, and Qingshi Zhu, Phys. Rev. Lett. **83**, 3001 (1999).

[45] J. I. Pascual, J. Gómez-Herrero, C. Rogero, A. M. Baró, D. Sánchez-Portal, E. Artacho, P. Ordejón, and J. M. Soler, Chem. Phys. Lett. **321**, 78 (2000). Part of Fig. 2 reprinted with permission from Elsevir, Copyright (2000).

[46] J. I. Pascual, J. Gómez-Herrero, A. M. Baró, D. Sánchez-Portal, E. Artacho, P. Ordejón, and J. M. Soler, Phys. Rev. Lett. **85**, 2653 (2000).